Point spread function computation in normal incidence for rough optical surfaces

Kashmira Tayabaly[1,2], Daniele Spiga[1], Giorgia Sironi[1], Michèle Lavagna[2], Giovanni Pareschi[1]

[1] INAF/Brera Astronomical Observatory, Via Bianchi 46, 23807 Merate, Italy
[2] Politecnico di Milano, Via La Masa 1, 20156 Milano, Italy

ABSTRACT

The Point Spread Function (PSF) allows for specifying the angular resolution of optical systems which is a key parameter used to define the performances of most optics. A prediction of the system's PSF is therefore a powerful tool to assess the design and manufacture requirements of complex optical systems. Currently, well-established ray-tracing routines based on a geometrical optics are used for this purpose. However, those ray-tracing routines either lack real surface defect considerations (figure errors or microroughness) in their computation, or they include a scattering effect modeled separately that requires assumptions difficult to verify. Since there is an increasing demand for tighter angular resolution, the problem of surface finishing could drastically damage the optical performances of a system, including optical telescopes systems. A purely physical optics approach is more effective as it remains valid regardless of the shape and size of the defects appearing on the optical surface. However, a computation when performed in the two-dimensional space is time consuming since it requires processing a surface map with a few micron resolution which sometimes extends the propagation to multiple-reflections. The computation is significantly simplified in the far-field configuration as it involves only a sequence of Fourier Transforms. We show how to account for measured surface defects and roughness in order to predict the performances of the optics in single reflection, which can be applied and validated for real case studies.

Keywords: PSF, surface metrology, physical optics, microroughness, scattering, Fourier transform, surface imperfections

1. INTRODUCTION

Optical systems are often characterized by their Point Spread Function (PSF). The PSF prediction from the surface metrology is a crucial step in the manufacturing process. It shows how much the surface finishing and the profile figuring should be pushed forward. The contributions of mirror surface imperfections to the PSF broadening are divided into shape errors and roughness. Shape errors cause distortions of the wavefront that can be predicted via geometric methods and roughness scatters the reflected light flux. These effects can be modeled using methods that depend on the spatial frequency classification.[1] The difficulty is trying to precisely define the spatial frequency regime in which each method (ray-tracing, first-order scattering theory, etc) can be adopted. There is no general consensus on this matter. An additional concern is how a combination of the PSFs resulting from imperfections in different spatial regimes should be performed. This situation prompts uncertainties and inconsistencies when simulating the PSF expected from a real mirror; therefore, mirror fabrication tolerances have to be established.

Surprisingly, a general unrestricted method to compute the PSF has been known for centuries: the Huygens-Fresnel principle. It is used in wavefront propagation techniques, but it has been seldom utilized to compute the PSF of real mirrors. As its validity is unrestricted, it does not require splitting a mirror profile into different spectral regimes. At first, the Huygens-Fresnel principle entails the numerical computation of complex 2D integrals over the mirror surface with a very tight sampling in order to account for mirror surface microroughness. Fortunately, there are two ways to simplify the numerical intensiveness of the computation:

contact author: E-mail: kashmira.tayabaly@brera.inaf.it, Telephone: +39 039 8943740

1. Working in grazing incidence geometry such as for X-ray mirrors, reduces the formalism to 1D[2,3]
2. Working in far-field approximation allows reducing the 2D Fourier integrals to the Fourier Transform which makes fast and efficient numerical algorithms.

A previous study set the foundation for generalizing this approach to the two-dimensional case.[4] We have introduced real surface imperfections (figure errors and microroughness) in this Physical Optics based simulation and successfully applied it to real case studies. The PSF of ASTRI-SST (Astrofisica con Specchi a Tecnologia Replicante Italiana- Small Size Telescope),[5] an Imaging Atmospheric Cherenkov Telescopes (IACT) mirror panel dedicated to the observation and study of γ-ray sources has been simulated and experimentally acquired for validation.

2. POINT SPREAD FUNCTION COMPUTATION IN FAR-FIELD APPROXIMATION

2.1 Review of single-reflection optical systems

Following the procedure based on the Huygens-Fresnel principle and developed[2] for the case of grazing-incidence mirrors, we adopt a reference frame as in Fig. 1, with the mirror profile described by the function $z_M(x_1,\, y_1)$, over a pupil M_1 of generic shape and size with area A_M. We select the origin of the reference frame setting $z_M(0,0)=0$. The source S, located at $(x_\mathrm{S},\, y_\mathrm{S},\, z_\mathrm{S})$, is assumed to be point-like and perfectly monochromatic of wavelength λ; hence, spatially and temporally coherent. The diffracted intensity is recorded at the position $\mathrm{P}(x_2,\, y_2,\, \bar{z_2})$, which may represent a location of either a detector array or the surface of the secondary mirror, if included in the optical layout. The detection array is parallel to the xy plane, at a constant height $\bar{z_2}$. Assuming that $\bar{z_2} \gg z_M$, $z_\mathrm{S} \gg z_M$ over the entire mirror map, and finally that $\bar{z_2}$ and z_S are much larger than the mirror lateral size. As fully demonstrated in,[4] this approximation enables the reduction of the Fresnel integrals to a Fourier Transform.

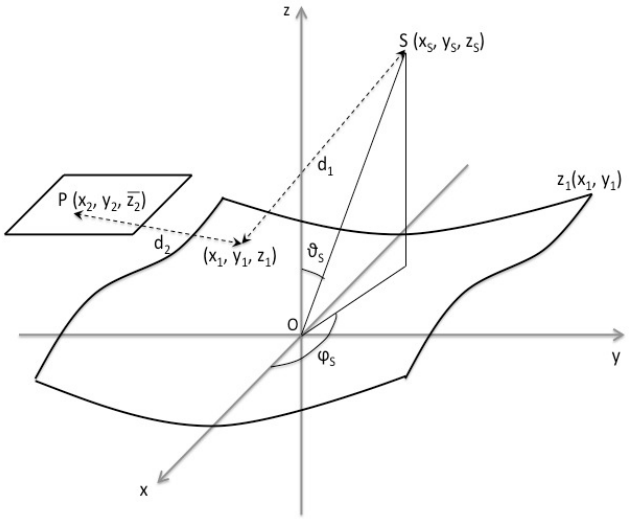

Figure 1. Scheme of computation for the electric field from the source S, diffracted by a mirror described by the profile $z_1(x_1, y_1) = z_M(x_1, y_1)$ at the $(x_2,\, y_2,\, \bar{z_2})$ location on the detection plane (or the secondary mirror surface). Polarization effects are not considered. The polar angles that locate the position of the detector are omitted to simplify the drawing.

Indeed, as per the Fresnel diffraction theory, the electric field at $(x_2,\, y_2,\, \bar{z_2})$ can be expressed as

$$E_2(x_2, y_2, \bar{z_2}) = \frac{E_0}{\lambda \bar{z_2}} \cos\theta_2 \, e^{-\frac{\pi \mathrm{i}}{\lambda z_2}(x_2^2+y_2^2)} \int_{\mathrm{M}_1} e^{\frac{4\pi \mathrm{i}}{\lambda}\Delta z_M} e^{2\pi \mathrm{i}(f_x x_1 + f_y y_1)} \, \mathrm{d}x_1 \mathrm{d}y_1, \tag{1}$$

where we have defined Δz_M as:

$$\Delta z_M = z_M(x_1, y_1) - \frac{x_1^2 + y_1^2}{4z_{\mathrm{R}}}, \tag{2}$$

i.e., the difference between a true mirror profile and a parabola with focal length of z_{R}, where

$$\frac{1}{z_{\mathrm{R}}} = \frac{1}{z_{\mathrm{S}}} + \frac{1}{\bar{z_2}}, \tag{3}$$

and the spatial frequencies are defined via the equations:

$$f_x = \frac{1}{\lambda}\left(\frac{x_2}{\bar{z_2}} + \frac{x_{\mathrm{S}}}{z_{\mathrm{S}}}\right), \qquad f_y = \frac{1}{\lambda}\left(\frac{y_2}{\bar{z_2}} + \frac{y_{\mathrm{S}}}{z_{\mathrm{S}}}\right). \tag{4}$$

The specular direction of the source is correctly defined as $x_2/z_2 = -x_{\mathrm{S}}/z_{\mathrm{S}}$, and similarly for y_2. In the case of a source at infinity, the spatial frequencies are defined as:

$$f_x^{\infty} = \frac{1}{\lambda}\left(\frac{x_2}{\bar{z_2}} + \sin\theta_{\mathrm{S}}\cos\varphi_{\mathrm{S}}\right), \qquad f_y^{\infty} = \frac{1}{\lambda}\left(\frac{y_2}{\bar{z_2}} + \sin\theta_{\mathrm{S}}\sin\varphi_{\mathrm{S}}\right), \tag{5}$$

where θ_{S} and φ_{S} are the zenithal and the azimuthal angle of the source, with respect to the origin of the reference frame (see Fig. 1).

Equation 1 is essentially the Fourier Transform of the Complex Pupil Function (CPF) defined below:

$$\mathrm{CPF}_1(x_1, y_1) = \chi_{\mathrm{M}}\, e^{\frac{4\pi \mathrm{i}}{\lambda}\Delta z_M}, \tag{6}$$

where χ_{M} is the characteristic function of the pupil. This quantity is conveniently referred to as the Optical Transfer Function,

$$\mathrm{OTF}_1(x_2, y_2) = \frac{1}{A_{\mathrm{M}}}\int_{-\infty}^{+\infty}\mathrm{d}y_1 \int_{-\infty}^{+\infty}\mathrm{d}x_1\, \mathrm{CPF}(x_1, y_1)\, e^{2\pi\mathrm{i}(f_x x_1 + f_y y_1)} \tag{7}$$

Note that the reference surface in the definition of Δz_1 is independent of the lateral position of the source.

Hence the derived PSF is given by

$$\mathrm{PSF}(x_2, y_2, \bar{z_2}) = \frac{A_{\mathrm{M}}}{\lambda^2 \bar{z_2}^2}|\mathrm{OTF}_1(x_2, y_2)|^2, \tag{8}$$

where we have assumed that the PSF is observed in the vicinities of the specular direction, and therefore $\theta_{\mathrm{S}} \simeq \theta_2$. The normalization factor ensures that the integrated PSF is normalized to 1:

$$\int_{-\infty}^{+\infty}\mathrm{d}y_2 \int_{-\infty}^{+\infty}\mathrm{PSF}(x_2, y_2)\,\mathrm{d}x_2 = 1. \tag{9}$$

This theory was applied to a real case study where we directly took into account the real surface profile of reflective optics to predict their PSF. To introduce surface roughness with a resolution on the order of magnitude of the micron over the full mirror (1m order of magnitude), it was necessary to reconstruct the surface roughness over the full mirror pupil.

2.2 PSF simulation accounting for microroughness

2.2.1 Total PSF computation

We considered that the surface topography of the mirror $z_M(x, y)$ could be decomposed into different contribution $z_n(x, y)$. This was given by the surface measurement with instruments sensitive to different ranges of spatial frequencies.

$$z_M(x,y) = \sum^{n} z_n(x,y) \tag{10}$$

In our case, we considered the geometrical surface topography $z_g(x,y)$ containing the theoretical shape of the mirror $z_{th}(x,y)$ and its figure errors $z_{fe}(x,y)$. $z_r(x,y)$ is the map containing the roughness information of the mirror.

$$z_M(x,y) = z_{th}(x,y) + z_{fe}(x,y) + z_r(x,y) \tag{11}$$

Then,from Eq. 6, we obtained a total CPF including roughness information such that:

$$CPF_{tot} = \chi_M \exp^{\frac{4\mathrm{i}\pi}{\lambda}(z_g(x,y) - \frac{x^2+y^2}{4z_R} + z_r(x,y))}, \tag{12}$$

As the OTF was defined as the Fourier Transform of the CPF, we have:

$$OTF_{tot} = \mathcal{F}[\chi_{\mathrm{M}}\, e^{\frac{4\pi\mathrm{i}}{\lambda}\Delta z_g}] \otimes \mathcal{F}[e^{\frac{4\pi\mathrm{i}}{\lambda}z_r}] \tag{13}$$

So, the total PSF_{tot} was given in the detector space (x_2, y_2)- as defined by Eq. 4- by:

$$PSF_{tot}(x_2,y_2) = \left|\mathcal{F}[\chi_{\mathrm{M}}\, e^{\frac{4\pi\mathrm{i}}{\lambda}\Delta z_g}](x_2,y_2) \otimes \mathcal{F}[e^{\frac{4\pi\mathrm{i}}{\lambda}z_r}](x_2,y_2)\right|^2 \tag{14}$$

As described in the following sections, the validation test of this Physical Optics approach was performed on ASTRI-M1 hexagonal mirror panel in the corona 3 region. It is referred as ASTRI-COR3 panel.

3. REAL CASE STUDY

3.1 ASTRI description

This theory was tested on a real mirror IACT mirror, one of the ASTRI-SST primary mirror's panels. ASTRI (Fig. 2, A) is a prototype for CTA-SST fully developed by INAF-OAB.[5] Its optical design is based on a Schwarzschild-Couder configuration with a F# of 0.5 and an equivalent focal length of 2150 mm. The M1 mirror is 4.02m in diameter, tessellated into hexagonal mirrors which face-to-face dimension is 849 mm. The M1 mirror is divided into 3 sections or 3 coronae, according to the distance of the center of the segment to the center of M1 (Fig. 2, B). Therefore, the closest segments (857 mm from the center of M1) belong to corona 1, mirrors placed 1485 mm from the center of M1 are in corona 2, and the farthest segments (1715 mm from the center of M1) are in corona 3.

The M1 mirror of ASTRI-SST is an aspherical mirror defined as:

$$z(r) = \frac{cr^2}{1+\sqrt{1-(cr)^2}} + \sum_{i=1}^{N} a_i r^{2i} \tag{15}$$

where $z(r)$ is the surface profile, r the surface radial coordinate, c the curvature and α_i the coefficients of asphericity detailed in Table. 1.

Each of the panels are cold slumped glass sandwich mirrors[6] : an Aluminum honeycomb structure is put in between two thin layers of glass coated with Aluminum and Quartz ($Al + SiO_2$) to ensure a lightweight mirror.

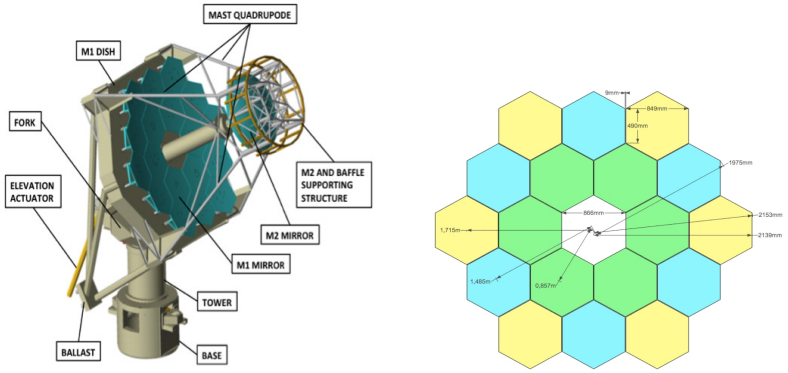

Figure 2. Optical design of ASTRI-SST (after[5]). A) 3D optical layout for ASTRI-SST 2M telescope. B) ASTRI-SST M1 tessellation. Green: corona 1. Blue: corona 2. Yellow: corona 3.

i	α
1	0
2	$9.61060 * 10^{-13}$
3	-5.6550110^{-20}
4	6.7798410^{-27}
5	3.8955810^{-33}
6	5.2803810^{-40}
7	-2.9910710^{-47}
8	$-4.39153 * 10^{-53}$
9	-6.1743310^{-60}
10	$2.73586 * 10^{-66}$

Table 1. Coefficients of asphericity for ASTRI-SST M1 mirror

4. SURFACE TOPOGRAPHY CHARACTERIZATION

4.1 Properties of various surface topography measurement instruments

Surface topography defects range from figure errors to surface finish, where each of the frequency regimes have a different impact on the PSF broadening.[1] The PSF prediction tool developed in this study can easily take into account all the surface defects regardless of the spatial frequency regime. The only remaining limitation is the resolution of the instrument used to measure the surface topography of the optics. Luckily, a combination of several instruments would cover different ranges from low to high spatial frequencies contents as described in Table 2.

Surface topography instruments	**Resolution**	**FOV**	**Technology**
UPMC	15 mm	full mirror	contact profilometry
Deflectometry	3 mm	full mirror	non-contact, surface slope error retrieval
MFT 2.5x	3.76 μm	$3.8 \times 2.9mm^2$	non-contact, optical microscopy
MFT 10x	0.93 μm	$0.95 \times 0.71mm^2$	non-contact, optical microscopy
AFM 100um	0.19 μm	$100 \times 100\mu m^2$	scanning probe microscope

Table 2. Surface Topography instruments and characteristics

4.2 Deflectometry for ASTRI-COR3

The low spatial frequency errors -i.e. figure errors- on ASTRI-COR3 surface panel were measured using the deflectometry technique developed in.[7] The retrieved maps from the slope error measurement setup shown

in Fig. 3A) had a Peak-to-Valley of 13mm and RMS of 2.5mm for ASTRI-COR3. The full mirror was not reconstructed because the discontinuities of the pupil made it difficult to properly retrieve the slope at the edges. Therefore, the retrieved pupil was $822mm \times 966mm$ instead of $849mm \times 980mm$ size of the full mirror, respectively in x and y direction. 500 Zernike terms were removed on the absolute surface mirror of ASTRI-COR3 in order to clearly reveal surface defects and particularly "the grid shape" error on the full panel area ($0.63m^2$) (Fig. 3B)). They are believed to be introduced by the honeycomb structure below the reflective layer of the mirror panel and could account for a poor image quality of optical systems. Using this real surface reconstruction, we simulated the pseudo-PSF (as defined in the next section) of this panel for different positions of the detector and compared them with real pseudo-PSF acquisition as shown in the next sections.

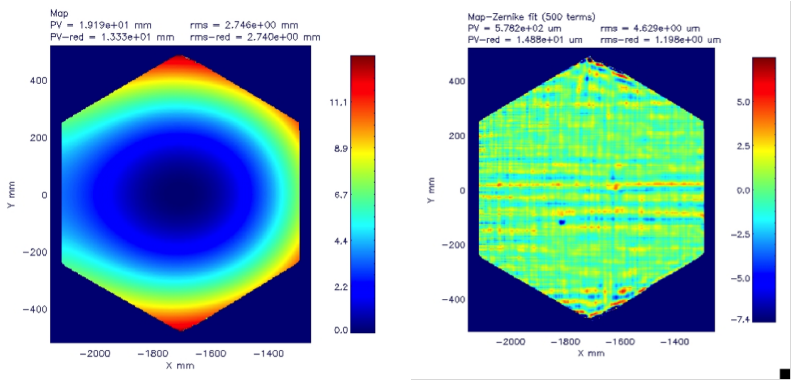

A B

Figure 3. Characterization of geometrical and figure error map obtained by deflectometry for ASTRI-COR3 panel: A)Surface Topography (in mm) B)Surface residual errors map measurement in mm panel corrected from 500 Zernike polynomials

5. PHYSICAL OPTICS PREDICTION VS EXPERIMENTAL PSF ACQUISITION

5.1 ASTRI pseudo-PSF

ASTRI is a double reflection aspheric telescope. There is no given focal point for its primary mirror M1 panels where the PSF could be found. Instead, we acquired the image of the mirror reflection in different image planes. We named those images pseudo-PSFs.

5.1.1 Setup for pseudo PSF acquisition

The experimental PSF is acquired using a setup developed at INAF-OAB and described in details in.[7] The setup consists of:

- **An optical bench** hosting the light source at 8430 mm from the center of the mirror.
- **A mirror support** composed of a mechanical support on top of a rotary table where the ASTRI-SST M1 panels are mounted, and where tip and tilt could also be adjusted. The rotary table allows the rotation of the mirror toward the optical bench and the screen. For our study, the hexagonal segment ASTRI-COR3 was mounted and oriented at 8.79° angle between the normal of the mirror at its center and the axis passing by the light source and the center of the mirror.
- **A screen** is mounted on a stage that allows moving the screen at different distances from the mirror.The pseudo-PSFs acquisition have been performed placing the screen at 4761 mm, 5794 mm, 7059 mm, 8183 mm, and 8840 mm from the mirror. The stage direction is aligned with the center of the rotary table at the basis of the mirror support by using a laser. The center of the rotary table is positioned on the barycenter of the obtained pattern.

Fig. 4 shows the setup configuration in 3D for experimental PSF acquisition. The facility uses a folding mirror to acquire distances perpendicularly to the optical axis and a camera is used to acquire pictures of the images reflected on the screen (see Fig. 5).

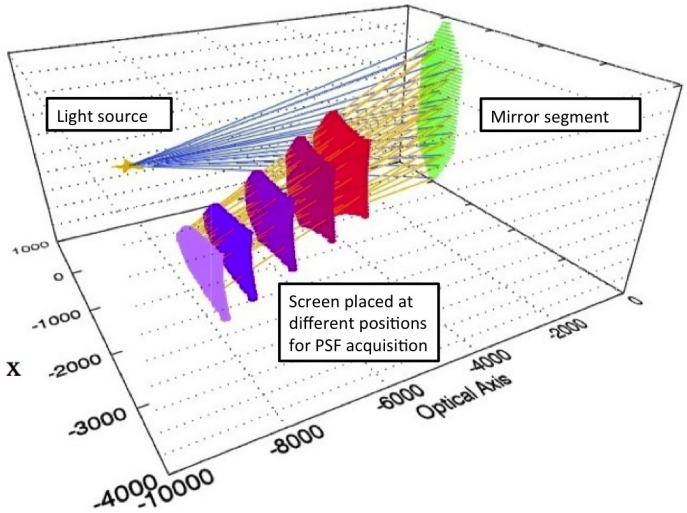

Figure 4. Setup for the experimental PSF acquisition of ASTRI-COR3 segment: a light source is at 8430 mm from the center of the mirror panel that is rotated at 8.79° off-normal, the reflected image from the mirror is acquired at various distances from its center (4761 mm, 5794 mm, 7059 mm, 8183 mm, and 8840 mm)

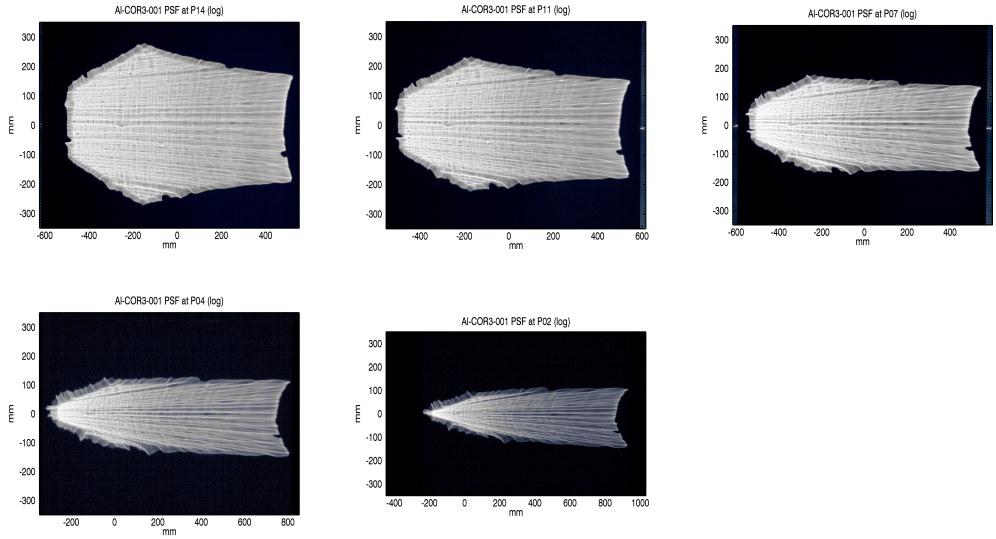

Figure 5. Image of the Pseudo-PSF of ASTRI-SST corona 3 segment acquired from the setup described in Fig.4: respectively from left to right $dist_{scr-mirr} = 4761\ mm, 5794\ mm, 7059\ mm$ on row 1, and $dist_{scr-mirr} = 8183\ mm, 8840\ mm$ on row 2

5.1.2 Pseudo-PSF simulation based on Physical Optics

The pseudo-PSF obtained from Physical Optics (PO) prediction used the theory expounded in Sect. 2. To decrease the computation time, the PO simulation considered the incoming light at $\lambda = 12\ \mu$m which was higher than the light source used in the experiment. This did not change the shape or the size of the pseudo-PSF, but enhanced the diffraction effect of the pupil taken into account with this method.

The results of the Physical Optics based simulation were compared to experimentally acquired pseudo-PSF of ASTRI-COR3 in the experimental setup described in Fig. 4. The results of the simulation are shown

in Fig. 6B) and Fig. 7. They were respectively comparable to experimentally obtained data displayed in Fig. 6A) and Fig. 5.

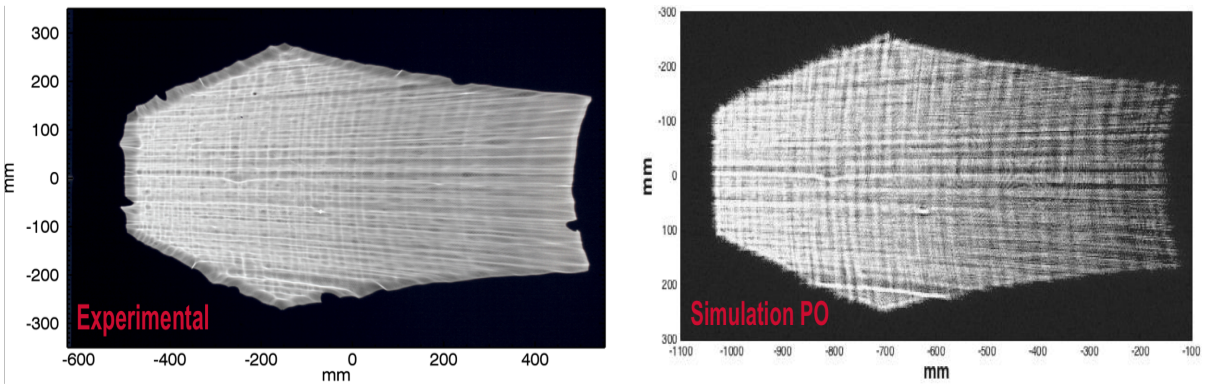

A B

Figure 6. Pseudo-PSF of ASTRI-SST corona 3 segment in the setup configuration described in in Fig.4 for a screen 4761mm away from the center of the mirror A)Pseudo-PSF experimentally acquired B)Pseudo-PSF simulated with the Physical Optics approach, $\lambda = 12\mu m$

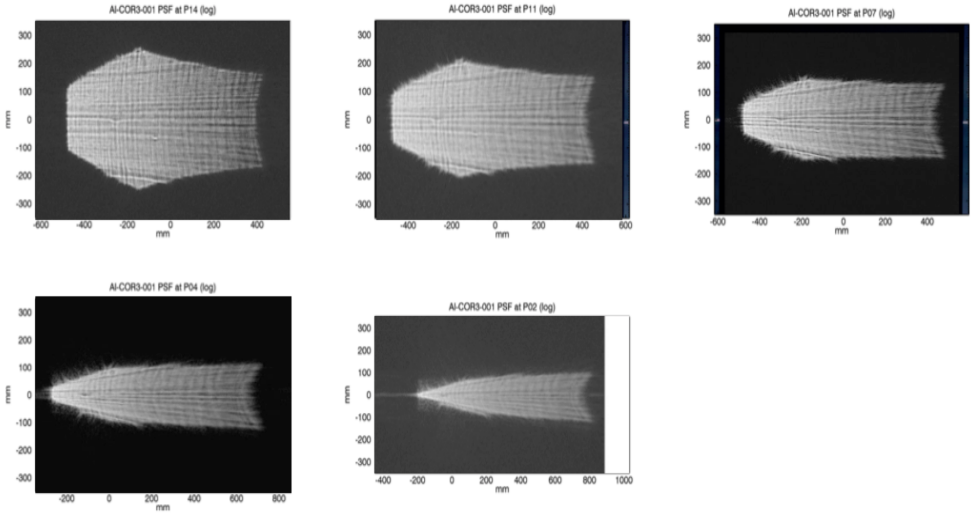

Figure 7. Image of the Pseudo-PSF of ASTRI-COR 3 segment simulated with the Physical Optics approach according to the setup described in Fig. 4: respectively from left to right $dist_{scr-mirr} = 4761\ mm, 5794\ mm, 7059\ mm$ on the first row, and $dist_{scr-mirr} = 8183\ mm, 8840\ mm$ on the second row

In order to compare the simulation, we took into account figure errors and the real experimental data in a quantitative way. We evaluated for each of these two approaches:

1. the size of the PSF in x direction as defined in Fig. 8 A), that we will call “xsize”.
2. the size of the PSF in y direction as defined in Fig. 8 A), that we will call “ysize”.
3. the distance between two defects pointed out in red in Fig. 8 B), that we will call “distance_def”.

As the distance between the mirror and the detector got longer, the pseudo-PSF became narrower in the y direction. This increased reading uncertainty in “ysize” . The simulation used a mirror map with a slightly underestimated size (1.5% to 3% underestimated), so “xsize” and “ysize” from the simulation were by default

smaller than for the experimentally acquired PSF. Consequently, we decided to compare the mapping of the defects on the pseudo-PSF and measured the distance between the two defects pointed in Fig. 8 B), whether it was simulated or experimentally acquired. Those defects were almost point like which provided better accuracy in their positioning and distance computation. Overcoming the uncertainty introduced by fuzzy edges and pupil size, it was undeniable that the simulation and the real experiment data matched perfectly, the ratio between the Simulation and the Experiment always remained higher than 89%, with a ratio of $100\% \pm 10\%$ for all the defects_dist data (see Table 3).

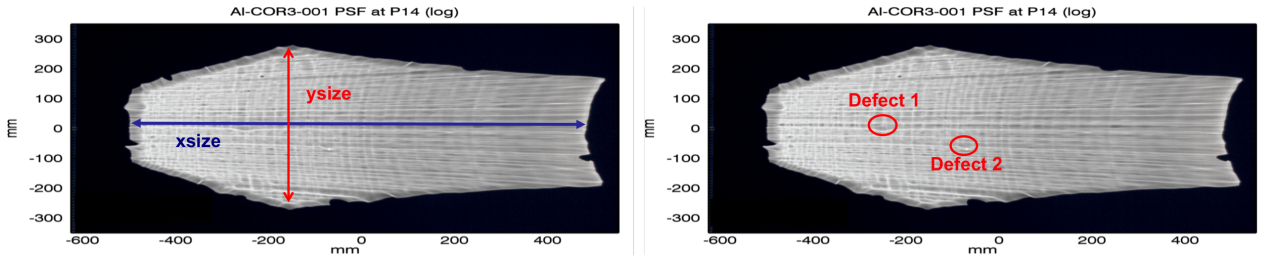

A B

Figure 8. Definition of parameters used for quantitatively comparing the PSF simulation based on Physical Optics and the real PSF for ASTRI-COR 3 panel, A) definition of xsize and ysize, B) definition of the defects considered for distance_def

Distance (mm)	Simulation			Experiment		
	xsize	ysize	distance_def	xsize	ysize	distance_def
4761	915.6	533.7	195.2	996.2	539.2	195.1
5794	945	425.8	185.8	1000	453.6	172.4
7059	945.1	308.7	180.4	996.6	346.2	168.4
8183	977.6	220.5	178.8	1062	240.8	168.6
8840	1009	175.8	171.9	1110	176.9	160.6

Table 3. Comparison of the absolute values simulated and experimentally acquired of ASTRI-COR3 segment's pseudo-PSF in the configuration described in Fig. 4 for xsize, ysize and distance_def

6. CONCLUSION

Using the Huygens-Fresnel principle, we have developed a way to successfully simulate the optical performances including real mirror surface defects over a broad range of spatial wavelengths (from a few μm to a few mm) for a near normal incidence, single reflection system. This approach was tested and validated in an out-of-focus configuration for the hexagonal and aspherical ASTRI-COR3 panel including shape errors. Not restricted to any spatial frequency regime, the developed technique is a powerful metrology tool to study various frequency regime contribution in surface scattering, either separately or combined, on reflective optics' performances. This would also help disentangling surface scattering contribution of various optical components in a complex optical system as often found in astronomical telescopes.

ACKNOWLEDGMENTS

This work is supported by the Italian National Institute of Astrophysics (INAF).

REFERENCES

1. J.E Harvey et al.",Total integrated scatter from surfaces with arbitrary roughness, correlation widths and incident angles", Opt. Engineering (2012)
2. Raimondi, L., Spiga, D., "Mirrors for X-ray telescopes: Fresnel diffraction-based computation of Point Spread Functions from metrology" Astronomy & Astrophysics, 573, A12 (2015)

3. Spiga, D., Raimondi, L., "X-ray optical systems: from metrology to Point Spread Function" Proc. SPIE 9209, 92090E (2014)
4. Tayabaly K, Spiga D, Sironi G., Canestrari R, Pareschi G, Lavagna, "Computation and validation of two-dimensional PSF simulation based on physical optics", SPIE 9577, 9577-8 (2015)
5. Pareschi, G., et al., "The dual-mirror Small Size Telescope for the Cherenkov Telescope Array", Procs. 33rd ICRC (2013)
6. Canestrari R., Pareschi G., Parodi F., Martelli F., Missaglia N., Banham R., "Cold shaping of thin glass foils as a method for mirror processing: from basic concepts to mass production of mirrors", Optical Engineering 52(5), 051204 (2013)
7. Sironi G., Canestrari R., Pareschi G. "Deflectometry for optics evaluation: Freeform segments of polynomial mirror", SPIE 91510T (2014)